Multi-time Scale Optimal Power Flow Strategy for Medium-voltage DC Power Grid Considering Different Operation Modes

Jianqiang Liu, Xiaoguang Huang, and Zuyi Li

***Abstract*—Direct current (DC) power grids based on flexible high-voltage DC technology have become a common solution of facilitating the large-scale integration of distributed energy resources (DERs) and the construction of advanced urban power grids. In this study, a typical topology analysis is performed for an advanced urban medium-voltage DC (MVDC) distribution network with DERs, including wind, photovoltaic, and electrical energy storage elements. Then, a multi-time scale optimal power flow (OPF) strategy is proposed for the MVDC network in different operation modes, including utility grid-connected and off-grid operation modes. In the utility grid-connected operation mode, the day-ahead optimization objective minimizes both the DER power curtailment and the network power loss. In addition, in the off-grid operation mode, the day-ahead optimization objective prioritizes the satisfaction of loads, and the DER power curtailment and the network power loss are minimized. A dynamic weighting method is employed to transform the multi-objective optimization problem into a quadratically constrained quadratic programming (QCQP) problem, which is solvable via standard methods. During intraday scheduling, the optimization objective gives priority to ensure minimum deviation between the actual and predicted values of the state of charge of the battery, and then seeks to minimize the DER power curtailment and the network power loss. Model predictive control (MPC) is used to correct deviations according to the results of ultra short-term load forecasting. Furthermore, an improved particle swarm optimization (PSO) algorithm is applied for global intraday optimization, which effectively increases the convergence rate to obtain solutions. MATLAB simulation results indicate that the proposed optimization strategy is effective and efficient.**

***Index Terms*—Optimal power flow (OPF), medium-voltage direct current (MVDC), quadratically constrained quadratic programming (QCQP), model predictive control (MPC), particle swarm optimization (PSO).**

I. Introduction

OVER the past decade, direct current (DC) power distribution techniques have developed rapidly. The remarkable technical advantages of DC distribution techniques can be applied for solving problems associated with conventional alternate current (AC) distribution networks. These problems include facilitating the large-scale integration of distributed energy resources (DERs), and improving power distribution capacities while reducing the need for additional power supply. However, DC power distribution networks must typically adopt various operation modes to accommodate different types of DERs and loads. Therefore, DC power distribution networks require advanced energy management. Optimal power flow (OPF) is the core component of advanced energy management systems (EMSs), with the important role of ensuring the economic, safe, and reliable operation of DC distribution networks [1]-[3].

Notable achievements have been made in the development of OPF strategies for DC power networks worldwide. For example, an adaptive particle swarm optimization (PSO) algorithm based on the fuzzy control theory was proposed for optimizing the power flow while considering both the active power losses and voltage quality [4]. A multi-time scale coordination scheduling method based on model predictive control (MPC) was proposed to address problems associated with the untimely response of unit regulation and large tracking errors [5]. A multi-stage dispatching method and source-network-load coordination strategy adopting the energy storage station (ESS) cost and operation cost as optimization objectives were developed for medium- and low-voltage microgrids [6]-[8]. Additionally, a variety of optimization algorithms have been studied separately and demonstrated to be feasible for conducting OPF using the distribution network power loss and operation cost as the optimization objectives [9]-[13]. These algorithms include the genetic algorithm (GA), the biogeography optimization algorithm [14], differential evolution, non-dominated sorting GA II (NSGA-II), mixed-integer nonlinear programming [15]-[21], the interior point method, and the conventional Lagrange multiplier algorithm. The optimization of the power flow was also conducted for independent microgrid systems using the operation cost of a microgrid and the emission cost as the optimization objectives, and the effects of employing an ESS on the optimization objectives were investigated [9]. The results indicated that both the operation and emission costs were reduced when the ESS was employed. The foregoing discussion indicates that previous research mainly focused on the mathematical model-

Manuscript received: November 14, 2018; accepted: May 28, 2019. Date of CrossCheck: May 28, 2019. Date of online publication: October 7, 2019.

This work was supported by Fundamental Research Funds for the Central Universities (No. 2019JBM057).

J. Liu (corresponding author) and X. Huang are with the School of Electrical Engineering, Beijing Jiaotong University, Beijing 100044, China (e-mail: liujianqiang@bjtu.edu.cn; huangxiaoguang80@163.com).

Z. Li is with the Robert W. Galvin Center for Electricity Innovation, Illinois Institute of Technology, Chicago 60616, USA (e-mail: lizu@iit.edu).

DOI: 10.35833/MPCE.2018.000781

ing, solving an algorithm, and scheduling characteristic improvement strategy for different optimization objectives of microgrid systems. Few studies have focused on adjustment and control strategies of multiple optimization objectives with consideration of the DC power station constraints and multiple operation modes.

To address the aforementioned issues, this study focused on multi-time scale and control problems of integrated multi-optimization objective for medium-voltage DC (MVDC) power grids with the multi-mode operation, employed for an urban power supply. According to the previous work [5], it is assumed that the DER power prediction error decreases with a decreasing prediction time scale. Therefore, in this study, the optimal scheduling of MVDC power grids is divided into two stages: day-ahead scheduling and the intraday rolling correction to mitigate the effect of intermittent DERs. In Section II, the topology and composition of a typical urban MVDC distribution network that includes a wind farm, a photovoltaic (PV) station, and an ESS are analyzed. Section III considers the output of DERs and power station converter constraints to model an optimal day-ahead dispatching objective according to the maximum utilization of DERs, minimum network power loss, and minimum load loss when the power supply is insufficient to satisfy the demand. The primary intraday dispatching optimization objectives are to minimize the deviations between the actual and predicted state of charge (SOC) values of the batteries in the ESSs and to minimize the deviations between the actual and predicted values of the total DER utilization and the total network power loss. In Section IV, the variable weight coefficient method is developed for the day-ahead optimization problem, which is consequently converted into a single-objective quadratically constrained quadratic programming (QCQP) problem to facilitate its solution. The influence of the system operation mode on the weight coefficients of multi-objective optimization is analyzed. Intraday optimization is implemented using an MPC rolling adjustment strategy developed to minimize the influence of uncertain power grid factors, and the MPC strategy is solved using an improved PSO algorithm. In Section V, MATLAB is employed to simulate and verify the operation mode and control strategy of the system proposed in Sections II, III, and IV. The final section concludes the paper.

II. Structure of Typed Urban MVDC Power Grid

This paper assumes a condition where a renewable-energy power-generation cluster exists near an urban center. It is assumed that the DER cluster can be connected to an MVDC distribution network in two possible ways: either as a medium-voltage power grid or as a low-voltage decentralized grid. The ±10 kV MVDC distribution network adopts the ring circuit structure shown in Fig. 1 composed of eight nodes denoted as P1-P8. The network accommodates the connection of both a large-capacity PV station (P6) and a wind farm (P3) and may include a DC converter station (P1) and an AC converter station (P8) that can be used to export renewable energy power or import power from other utility grids. Low-voltage inverters are distributed as small power grid-connected devices in a ±750 V low-voltage DC (LVDC) microgrid. The MVDC distribution network accommodates two load types: a unidirectional power flow load and a bidirectional power flow load. All loads are connected to the DC distribution network by buck converter stations. The loads include a subway power station (P2), an ESS station (P5), an LVDC industrial park power station (P7), and a residential area power station (P4). The power and load conditions in the assumed scenario are presented in Appendix A Table AI and are derived from a standard IEEE 13-node distribution network after adjustment. In this scenario, when the MVDC operates in utility grid-connected mode, the absorption and delivery of DER power generation are the main control targets. When the MVDC operates in the off-grid operation mode, the supply safety of the loads is the main control target.

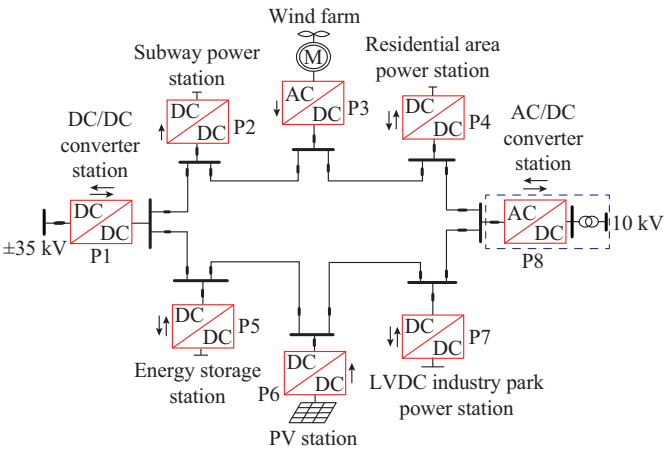

Fig. 1. Topology of assumed MVDC distribution network.

III. Model and Management of Optimization Target

A. Day-ahead Optimization Model

In the utility grid-connected mode, the maximum DER utilization and minimum network power loss are taken as the optimization objectives. In the off-grid or islanded operation mode, the primary objective is to minimize the load loss, and the secondary objective is to minimize the DER curtailment and network power loss.

1) DER Utilization Index

To simplify the optimization problem for day-ahead scheduling over a period T, the standard objective of maximum DER utilization is replaced with the objective of minimum DER power curtailment in the present study. The total DER power curtailment D_{loss} is expressed as follows:

$$D_{loss} = \sum_{i=1}^{N}\sum_{t=1}^{T}\left(P_{DERi,\max}(t) - P_{DERi}(t)\right) \tag{1}$$

where $P_{DERi}(t)$ is the active power output; $P_{DERi,\max}(t)$ is the predicted active power output of the i^{th} DER over the t^{th} time interval; and N is the number of DERs.

2) Network Power Loss Index

The network power loss index P_{loss} is calculated as follows:

$$P_{loss} = \sum_{t=1}^{T} \sum_{(i,j) \in I} G_{ij} \left(V_i^t - V_j^t \right)^2 \tag{2}$$

where G_{ij} is the line admittance from node i to node j; and V_i^t and V_j^t are the voltages of nodes i and j, respectively, in the t^{th} time interval for a total of I lines.

3) Load Loss Index

The total load loss L_{loss} is calculated as follows:

$$L_{loss} = \sum_{t \in T} \sum_{i \in L} \left(P_i^p(t) - P_i(t) \right) \tag{3}$$

where $P_i^p(t)$ is the predicted power; and $P_i(t)$ is the actual power of load i in the t^{th} time interval for a total of L loads.

The optimization of day-ahead scheduling can be defined by combining (1)-(3) as follows:

$$\min \left(\lambda_1 k_1 D_{loss} + \lambda_2 k_2 P_{loss} + \lambda L_{loss} \right) \tag{4}$$

where the weight coefficients λ_1 and λ_2 are in the range [0, 1] ($\lambda_1 + \lambda_2 = 1$ must be satisfied); k_1 and k_2 are the normalization coefficients; and λ is the load loss coefficient, which is set as 0 when the network functions in the utility grid-connected operation mode. When the network functions in the off-grid operation mode, we set $\lambda \gg \lambda_1 k_1 + \lambda_2 k_2$.

B. Intraday Optimization Model

As previously discussed, the primary intraday dispatching optimization objective is to minimize the deviations between the actual and predicted SOC values of the N_{ES} batteries in the ESS and to minimize the deviations between the actual and the predicted values of D_{loss} and P_{loss}, so that the optimization results approach the day-ahead comprehensive optimization goal. We adopt MPC to perform rolling optimal scheduling based on ultra-short-term DER predictive data to suppress the effects of various uncertainties on the optimization objectives. The intraday dispatching objective function is as follows:

$$\min \left[\beta_1 \sum_{t=t_0}^{t_0+T} \sum_{i=1}^{N_{ES}} \left| S_{Ei}(t) - S_{Ei}^p(t) \right| + \beta_2 \left(\frac{D_{loss} - D_{loss}^p}{D_{loss}^p} + \frac{P_{loss} - P_{loss}^p}{P_{loss}^p} \right) \right] \tag{5}$$

where β_1 and β_2 are the optimal weight coefficients, they are in the range [0, 1] and must satisfy $\beta_1 + \beta_2 = 1$; $S_{Ei}(t)$ is the ultra-short-term forecasting data; $S_{Ei}^p(t)$ is the day-ahead predicted value for the SOC of the i^{th} battery of the ESS in the t^{th} time interval; and D_{loss}^p and P_{loss}^p are the day-ahead predicted values of D_{loss} and P_{loss}, during the period of t_0 to $t_0 + T$, respectively. We define $\beta_1 > \beta_2$ to make the first term of the objective function in (5) to be the primary optimization goal for ensuring that the ESS satisfies the energy balance constraint of daily operation and that the second term of the objective function is a sub-optimization objective.

C. Constraint Conditions

1) Power Flow Equation Constraints

Ignoring the loss of power and loads at the grid-connected interface converters and assuming that power nodes are equalized by the DC injection power and that the load nodes conform to a constant-power model, the power flow equation is constrained as follows:

$$\begin{cases} I_{ij}^t = G_{ij} \left(V_i^t - V_j^t \right) \\ P_{cvi}^t = V_i^t \sum_{j=1}^{n} G_{ij} V_j^t \\ P_{cvi}^t = P_{DERi}^t + P_{uti}^t + P_{ESi}^t - P_{Li}^t \\ V_{i,\min} \le V_i \le V_{i,\max} \end{cases} \tag{6}$$

where $t \in \{1, 2, ..., T\}$; $i,j \in \{1, 2, ..., I\}$; I_{ij}^t is the line current from node i to node j in the t^{th} time interval; P_{cvi}^t is the converter output power of the i^{th} node in the t^{th} time interval; P_{uti}^t is the exchange power from the utility grid in the t^{th} time interval, $P_{uti}^t > 0$ represents power flow from the utility grid, and $P_{uti}^t < 0$ represents power flow to the utility grid; P_{ESi}^t is the power state of the i^{th} battery of the ESS in the t^{th} time interval, $P_{ESi}^t > 0$ represents a discharging state, and $P_{ESi}^t < 0$ represents a charging state; P_{Li}^t is the power of the i^{th} load in the t^{th} time interval; and $V_{i,\max}$ and $V_{i,\min}$ are the maximum and minimum voltages of the i^{th} node, respectively.

2) Power Boundary Constraints

$$P_{cvi,\min} \le P_{cvi}^t \le P_{cvi,\max} \tag{7}$$

$$P_{DERi,\min} \le P_{DERi}^t \le P_{DERi,\max} \tag{8}$$

where $P_{cvi,\min}$ and $P_{cvi,\max}$ are the minimum and maximum power outputs of the i^{th} converter, respectively; and $P_{DERi,\min}$ and $P_{DERi,\max}$ are the minimum and maximum active power outputs of the i^{th} DER, respectively.

3) Power Quality Constraints

The DC power flow can be controlled by node-voltage regulation. However, voltage regulation at any node causes uneven fluctuations in the network voltage distribution. Therefore, voltage distribution imbalances can be used to evaluate the voltage distribution and voltage control effect of the network [15]. For a network consisting of n nodes, the degree of voltage distribution imbalance D can be defined as the difference between the average of the squared node-voltage values (i.e., $E(V^2)$) and the squared average of the node-voltage values (i.e., $E(V)^2$), as follows:

$$D = E\left(V^2\right) - E\left(V\right)^2 = \frac{V_1^2 + V_2^2 + \ldots + V_n^2}{n} - \left(\frac{V_1 + V_2 + \ldots + V_n}{n} \right)^2 \le \epsilon \tag{9}$$

4) SOC Constraint of ESS

$$SOC_{ESi,\min} \le SOC_{ESi}^t \le SOC_{ESi,\max} \tag{10}$$

$$SOC_{ESi}^{t+1} = \left(1 - \eta_{ESi}\right) \cdot SOC_{ESi}^t - \frac{P_{ESi}^t \Delta T}{C_{ESi}} \tag{11}$$

$$SOC_{ESi}^T = SOC_{ESi}^1 \tag{12}$$

where SOC_{ESi}^t is the SOC of the i^{th} battery of the ESS in the t^{th} time interval; $SOC_{ESi,\max}$ and $SOC_{ESi,\min}$ are the maximum and minimum allowable SOC values of the i^{th} battery of the ESS, respectively; η_{ESi} is the self-discharge efficiency of the i^{th} battery of the ESS; ΔT is the duration of each time interval; and C_{ESi} is the capacity of the i^{th} battery of the ESS. Equation (10) gives the charging and discharging limits of a battery in the ESS. Equation (11) represents the time-series

SOC relationships for the batteries of the ESS. Equation (12) gives the daily conservation requirements for the batteries of the ESS, where the final SOC at $t = T$ must be equivalent to the initial SOC at $t = 1$ for each battery in the ESS.

5) Power Station Regulation Margin Constraint

The maximum power output of a power station is always limited by the maximum dispatching power of a connected utility grid used as the balancing node. Additionally, the output power of DERs and the ESS must be regulated to ensure the stable operation of the system. The maximum rate of change in the output power of a power station should be set with consideration of the power grid security and stability. Assuming that the range of fluctuation for the power output of a power station in the t^{th} time interval is $(-\Delta P^t, +\Delta P^t)$, the regulation margin of the power station is expressed as follows:

$$\alpha - \Delta P^t \le P^p_{uti}(t) \le \alpha + \Delta P^t \tag{13}$$

where α is the switching power dispatching value of the utility grid in the t^{th} time interval; and $P^p_{uti}(t)$ is the predicted output power of the i^{th} power station in the t^{th} time interval.

D. Optimization Target Management

The power difference between the supply and demand at any time t depends on the power status of loads, DERs, ESSs, and the utility grid in the power distribution system, as follows:

$$P_{\Delta}(t) = P_L(t) - \left(P_{DER}(t) + P_{BES}(t) + P_{GCC}(t)\right) \tag{14}$$

where $P_L(t)$ is the total power of the loads, which is equal to the sum of the power consumptions at P2, P4, and P7 in Fig. 1; $P_{DER}(t)$ is the total output power of the DERs, which is the sum of the power outputs at P3 and P6 in Fig. 1; and $P_{BES}(t)$ and $P_{GCC}(t)$ are the total ESS power output at P5 and the utility grid-connected converter (UGCC) power output at P8, respectively. As indicated by (14), $P_{\Delta}(t) = 0$ represents the energy equilibrium status of the system, $P_{\Delta}(t) > 0$ represents a state of insufficient power supply, and $P_{\Delta}(t) < 0$ represents a state of excess power supply.

From this perspective, the MVDC distribution system operation can be divided into the six operation modes listed in Table I, according to the statuses determined by $P_{\Delta}(t)$ and $P_{GCC}(t)$. The weight coefficients assigned to the optimization objectives can then be adjusted according to the operation mode evaluated in advance, which can ensure that the distribution system will function optimally. Detailed descriptions of each operation mode are presented as follows.

In mode 1, the UGCC is online (i.e., $P_{GCC}(t) \neq 0$), and $P_{DER}(t)$ can supply both $P_L(t)$ and ESS charging demand (i.e., $P_{\Delta}(t) = 0$). Therefore, the MVDC network does not need to exchange power with the utility grid. The UGCC is used as a balancing node, and the DERs operate in the maximum power point tracking (MPPT) mode. Because distributed generation can be fully absorbed, minimizing P_{loss} can be taken by the EMS as the main optimization goal.

In mode 2, $P_{GCC}(t) \neq 0$, and $P_{DER}(t)$ exceeds $P_L(t)$ and the ESS charging demand (i.e., $P_{\Delta}(t) < 0$). Here, the MVDC network must export power to the utility grid and/or charge the ESS. The UGCC is used as a balancing node, and the DERs operate in the MPPT mode. The EMS should consider minimizing D_{loss} and P_{loss} as the comprehensive optimization objective. However, if the power margins of the ESS and the utility grid are insufficient for absorbing the available excess power, the DERs must operate in the limited power mode.

In mode 3, $P_{GCC} \neq 0$, and $P_{DER}(t)$ is insufficient to satisfy $P_L(t)$ and the ESS charging demand (i.e., $P_{\Delta}(t) > 0$). In this case, the MVDC network must obtain power from the utility grid and/or discharge the ESS. The UGCC is used as a balancing node, and the DERs operate in the MPPT mode. The EMS should consider minimizing L_{loss} and P_{loss} as the comprehensive optimization objective. If the power margins of the ESS and the utility grid are insufficient to supply the required power, loads must be abandoned according to their priority.

In mode 4, the UGCC is offline (i.e., $P_{GCC}(t) = 0$), and $P_{\Delta}(t) = 0$. The ESS is used as a balancing node, and the DERs operate in the MPPT mode. Again, the EMS takes minimizing P_{loss} as the main optimization objective under the balanced supply and demand condition.

In mode 5, $P_{GCC}(t) = 0$, and $P_{\Delta}(t) < 0$. Here, the MVDC power grid must charge the ESS. The ESS is used as a balancing node, and the DERs operate in the MPPT mode. The EMS should consider minimizing D_{loss} and P_{loss} as the comprehensive optimization objective. If the power margin of the ESS is insufficient for absorbing the available excessive power, the DERs must operate in the limited power mode.

In mode 6, $P_{GCC}(t) = 0$ and $P_{\Delta}(t) > 0$. Here, the MVDC power grid must discharge the ESS. The ESS is used as a balancing node, and the DERs operate in the MPPT mode. The EMS should consider L_{loss} and P_{loss} as the comprehensive optimization objectives. If the power margin of the ESS is insufficient to supply the required power, loads must be abandoned according to their priority.

TABLE I
MAIN OPTIMIZATION OBJECTIVES IN DIFFERENT OPERATION MODES DEFINED ACCORDING TO (14)

Model	Status	Optimization target	Balance node
1	$P_{\Delta}(t) = 0$, $P_{GCC} \neq 0$	Minimize network power loss	UGCC
2	$P_{\Delta}(t) < 0$, $P_{GCC} \neq 0$	Minimize network power loss and DER curtailment	UGCC
3	$P_{\Delta}(t) > 0$, $P_{GCC} \neq 0$	Minimize load loss and network power loss	UGCC
4	$P_{\Delta}(t) = 0$, $P_{GCC} = 0$	Minimize network loss	ESS
5	$P_{\Delta}(t) < 0$, $P_{GCC} = 0$	Minimize network power loss and DER curtailment	ESS
6	$P_{\Delta}(t) > 0$, $P_{GCC} = 0$	Minimize load loss and network power loss	ESS

IV. Solution Strategy

A. Day-ahead Scheduling Algorithm

The day-ahead scheduling model presents a multi-objective QCQP problem. For such problems, NSGA-II and the multi-objective evolutionary algorithm are commonly used. However, these algorithms are time-consuming and cannot guarantee that a subset of the Pareto-optimal solution set is obtained. Therefore, in the present study, a multi-objective optimization algorithm based on dynamic weights is used to eliminate dimensional differences between the respective optimization objectives. This approach allows the original multi-objective QCQP problem to be decomposed into two steps involving the calculation of weights and the single-objective optimization. Taking the optimization presented in (4) for MVDC network operation in the grid-connected operation mode as an example, the first step is to calculate the normalization coefficients (k_1 and k_2) as follows:

1) Set $\lambda_1 = 1$ and $\lambda_2 = 0$. The minimum D_{loss} is the optimization objective. According to the optimization results, the minimum DER power curtailment D_{loss1} and the minimum network power loss P_{loss1} are obtained.

2) Set $\lambda_1 = 0$ and $\lambda_2 = 1$. The minimum P_{loss} is the optimization objective. According to the optimization results, the minimum DER power curtailment D_{loss2} and the minimum network power loss P_{loss2} are obtained.

3) Calculate $k_1 = P_{loss1} - P_{loss2}$ and $k_2 = D_{loss1} - D_{loss2}$.

The second step is to solve the single-objective optimization problem.

B. MPC Solution for Intraday Scheduling

As previously discussed, intraday optimization is implemented using an MPC rolling adjustment strategy developed to minimize the influence of uncertain power grid factors. This is achieved by adopting a primary intraday dispatching optimization objective that seeks to minimize deviations between the actual and predicted SOC values of the batteries in ESSs and to minimize the deviations between the actual and predicted values of total DER utilization and the total network power loss. MPC is a closed-loop optimization control method. The core idea of the algorithm is the receding horizon strategy [5]. To eliminate deviations between the actual and the predicted values caused by prediction error, the intraday EMS conducts rolling optimization and correction over 15 min cycles. Therefore, the ESS daily energy balance given by (12) can be ensured, and the day-ahead predicted switching power values of the utility grid can be tracked precisely.

The state vector of k moments is given as $\boldsymbol{X}(k) = [P_f(k), S_B(k), P_B(k)]^{\mathrm{T}}$ and includes the switching power of the utility grid $P_f(k)$, the SOC of the ESS $S_B(k)$, and the adjustable power of the MVDC distribution network $P_B(k)$. The control variable is defined as $u(k) = \Delta P_B(k)$, where $\Delta P_B(k)$ is the output power of the ESS. The disturbance variable is $\boldsymbol{r}(k) = [\Delta P_L(k), \Delta P_D(k)]$, which includes the forecasting increments in the load power $\Delta P_L(k)$ and in the DER output power $\Delta P_D(k)$. The output vector is $\boldsymbol{y}(k) = [\Delta P_L(k), \Delta S_B(k)]$. The multi-input multi-output state vector equation is given as follows:

$$\boldsymbol{X}(k+\Delta t) = \begin{bmatrix} P_f(k+\Delta t) \\ S_B(k+\Delta t) \\ P_B(k+\Delta t) \end{bmatrix} = \begin{bmatrix} 1 & 0 & 0 \\ 0 & 1-\eta & -\dfrac{\Delta t}{E_B} \\ 0 & 0 & 1 \end{bmatrix} \begin{bmatrix} P_f(k) \\ S_B(k) \\ P_B(k) \end{bmatrix} + \begin{bmatrix} 0 \\ 0 \\ -\dfrac{\Delta t}{E_B} \end{bmatrix} \Delta P_{\mathrm{B}}(k) + \begin{bmatrix} 1 & -1 \\ 0 & 0 \\ 0 & 0 \end{bmatrix} \begin{bmatrix} \Delta P_L(k) \\ \Delta P_D(k) \end{bmatrix} \tag{15}$$

$$\boldsymbol{y}(k) = \begin{bmatrix} P_f(k) \\ S_B(k) \end{bmatrix} = \begin{bmatrix} 1 & 0 & 0 \\ 0 & 0 & 1 \end{bmatrix} \begin{bmatrix} P_f(k) \\ S_B(k) \\ P_B(k) \end{bmatrix} \tag{16}$$

where Δt is the predicted interval; η is the battery self-discharge coefficient; and E_B is the battery capacity. As indicated by (15) and (16), the state space prediction model can be subjected to forward iteration by an arbitrary number (p) of predictive steps according to the ultra-short-term power prediction data of DER outputs and loads to obtain the following predictive vector $\boldsymbol{Y}_f$, which includes the values of $P_f^f(k)$ and $S_B^f(k)$ over a prediction interval Δt.

$$\begin{aligned} \boldsymbol{Y}_f = [\ & P_f^f(k+\Delta t) \quad S_B^f(k+\Delta t) \quad \cdots \\ & P_f^f(k+p\Delta t) \quad S_B^f(k+p\Delta t)\ ]^{\mathrm{T}} \end{aligned} \tag{17}$$

During the next $p\Delta t$ period, the vector shown in (18) is taken as the tracking control vector based on the forecasted values of $P_f^r(k)$ and $S_B^r(k)$. The objectives are to minimize the error $|\boldsymbol{Y}_r - \boldsymbol{Y}_f|$ and to minimize D_{loss} and P_{loss}, whereby the rolling optimization can be converted into the minimization problem defined by (5). An improved PSO algorithm presented in the following subsection is used to solve the optimization function. Subsequently, the optimal power instructions of all power stations can be obtained for the next $p\Delta t$ intervals. However, the scheduling system presently only dispatches instructions for the next scheduling cycle, and the foregoing rolling optimization process is repeated for each subsequent scheduling cycle.

$$\begin{aligned} \boldsymbol{Y}_r = [\ & P_f^r(k+\Delta t) \quad S_B^r(k+\Delta t) \quad \cdots \\ & P_f^r(k+p\Delta t) \quad S_B^r(k+p\Delta t)\ ]^{\mathrm{T}} \end{aligned} \tag{18}$$

C. Intraday Scheduling Algorithm

The optimal intraday scheduling model presents a nonconvex nonlinear optimization problem. Because the conventional approach employing the gradient descent algorithm suffers from the difficulty of finding the global optimum, an improved PSO algorithm is developed for conducting global optimization in the present study. The PSO algorithm is an intelligent optimization approach that relies on a large group of particles, each with an individual position x, representing parameters providing a solution to the optimization problem as well as a corresponding particle velocity v representing the speed at which the particle moves through the solution space. The updating formula is given as follows:

$$x \leftarrow x + v \tag{19}$$

$$v \leftarrow \Omega v + c_1 r_1 (x_p - x) + c_2 r_2 (x_g - x) \tag{20}$$

where Ω is the inertia coefficient; c_1 and c_2 are the group learning coefficients; r_1 and r_2 are the random numbers in the range [0, 1]; x_p is the best position that a particle has found thus far; and x_g is the best position found by the group of particles thus far, where $x_g = \min(x_p)$.

However, the conventional PSO algorithm is easily trapped in local optima because of its fixed parameters. In the present study, this tendency is mitigated by introducing a compression factor ϕ and replacing Ω with an adaptive inertia coefficient ω. First, we define ϕ as follows:

$$\phi = \frac{c - 2 - \sqrt{4c - c^2}}{2} \tag{21}$$

where $c = c_1 + c_2$. Equation (20) is revised as follows:

$$v \leftarrow \frac{\omega v + c_1 r_1 \left(x_p - x\right) + c_2 r_2 \left(x_g - x\right)}{\phi} \tag{22}$$

The significance of ϕ is to limit the maximum values of c_1 and c_2, reducing the probability of oscillation during the optimization process. Then, we define ω as follows:

$$\omega = \begin{cases} \omega_{\min} - \dfrac{\left(\omega_{\max} - \omega_{\min}\right)\left(f - f_{\min}\right)}{f_{\text{avg}} - f_{\min}} & f \le f_{\text{avg}} \\ \omega_{\max} & f > f_{\text{avg}} \end{cases} \tag{23}$$

$$\begin{cases} f_i = |Y_r(i) - Y_f(i)| + D_{loss}(i) + P_{loss}(i) \\ f_{\min} = \min\left(f_1, f_2, \ldots, f_n\right) \\ f_{\text{avg}} = \dfrac{1}{n}\sum_{i=1}^{n} f_i \end{cases} \tag{24}$$

where n is the number of parcels; and f_i is the fitness value of the i^{th} parcel, with $i \in n$.

The significance of ω is to balance the local search and global search abilities of the particle swarm. When the fitness value of a particle f is less than the average of the population f_{avg}, ω is reduced, and the global search ability of the particle swarm is correspondingly enhanced. The minimum value of ω is set to $\omega_{\min}$. In contrast, when $f > f_{\text{avg}}$, the maximum inertia $\omega_{\max}$ is used and the local searchability of the particle swarm is enhanced. A flowchart of the improved PSO algorithm is shown in Fig. 2.

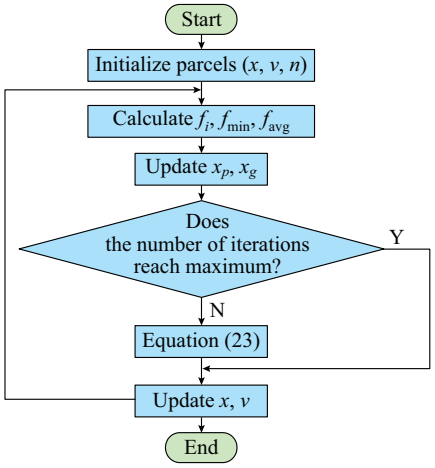

Fig. 2. Flowchart of improved PSO algorithm.

V. Simulation and Analysis

According to the distribution network topology shown in Fig. 1, the power and load conditions used in the simulation are presented in Appendix A Table AI, and the MVDC network line parameters are presented in Appendix A Table AII. The benchmark of power grid capacity is 100 MVA. The day-ahead and intraday forecast data for the DERs and loads are shown in Appendix B Figs. B1 and B2, respectively. The self-discharge rate of the ESS is set as 0.01.

A. Analysis of Day-ahead Scheduling Results

The FMINCON solver provided in the YALMIP environment of MATLAB is employed to solve the single-objective QCQP problem. The optimization results obtained for the MVDC power distribution grid in the utility grid-connected operation mode using fixed weight coefficients ($\lambda_1 = \lambda_2 = 0.5$) are shown in Fig. 3(a). A total DER curtailment of 31.9892 MWh and a total power net loss 0.003 MWh are obtained. The optimization results obtained by dynamically adjusting the weight coefficients using the strategy proposed in Section IV-A ($\lambda_1 = 0.9$, $\lambda_2 = 0.1$) are shown in Fig. 3(b). Here, a total DER curtailment of 0.3861 MWh and a total power net loss 0.0048 MWh are obtained.

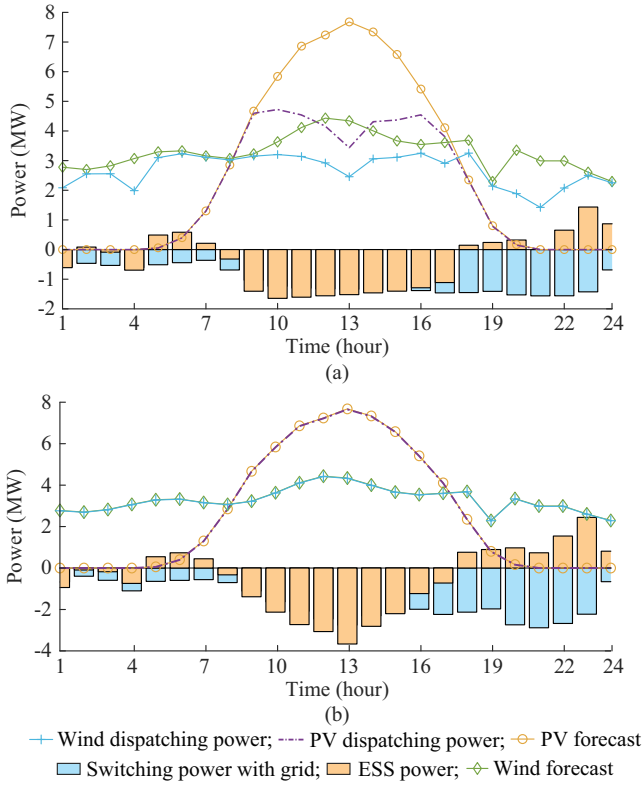

Fig. 3. Optimization results for different weight coefficients in utility grid-connected operation mode. (a) $\lambda_1 = 0.5$, $\lambda_2 = 0.5$. (b) $\lambda_1 = 0.9$, $\lambda_2 = 0.1$.

The simulated PV power curves indicate that a contradictory relationship exists between P_{loss} and D_{loss}, i.e., a decrease in P_{loss} leads to an increase in D_{loss} and vice versa. Even under the conditions of a DER surplus, the optimal results obtained using fixed weight coefficients in Fig. 3(a) result in large-scale DER curtailment. However, as shown in Fig. 3(b),

this problem is mitigated by adjusting the weight coefficients according to the forecasting data. The switching power curves show that increasing the switching power with the utility grid is helpful for reducing the network power loss, but it reduces the DER utilization. The ESS power curves in Fig. 3 show that the role of the ESS is to stabilize fluctuations in the renewable-energy outputs, and the larger weight coefficient governing the DER utilization objective increases the ESS utilization rate. Additionally, as shown in Appendix B Fig. B3, the voltage fluctuations of the nodes are controlled below 1% for weight-coefficient settings of $\lambda_1 = \lambda_2 = 0.5$ and $\lambda_1 = 0.9$, $\lambda_2 = 0.1$, which satisfies the power quality requirements. However, the larger weight coefficient governing the net power loss optimization objective provides a smaller voltage fluctuation range.

The optimization results for the MVDC power distribution grid in the off-grid operation mode obtained by dynamically adjusting the weight coefficients using the strategy proposed in Section III-A are presented in Fig. 4. The charging and discharging frequencies and depths of the ESS are greater than those obtained for the MVDC power distribution grid in the utility grid-connected operation mode. This is mainly because the ESS serves as the balancing node of the MVDC power distribution grid when the utility grid is not connected.

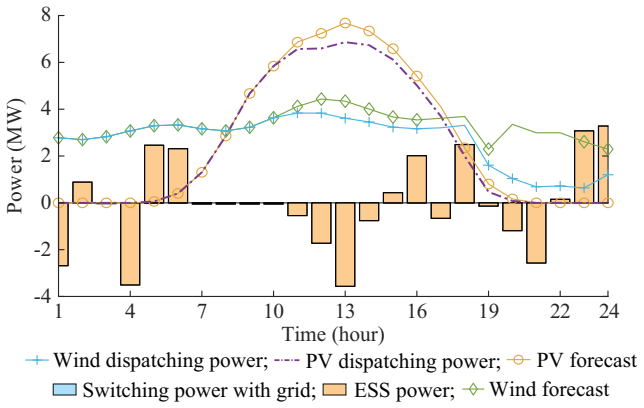

Fig. 4. Optimization results for off-grid operation mode.

B. Intraday Scheduling Results

To analyze the proposed intraday scheduling approach, we employ an MPC predictive time scale of 1 hour and a rolling dispatching period of 15 min. The population size of the particle swarm is 40, $c_1 = c_2 = 2$, and the maximum number of iterations is 200. As shown in Fig. 5, the convergence rate of the improved PSO was significantly higher than that of the classical PSO. The improved PSO obtained a global optimum value of 0.0762 in the 20th iteration, whereas the classical PSO is trapped in a local optimum value of 342.9837. This example indicates that the dynamic inertia weight proposed in this paper helps the PSO to avoid falling into local optima.

In this case, the relative error of the DERs between the ultra-short-term prediction and the day-ahead prediction is 21.8%. As shown in Fig. 6, the total relative deviations between the day-ahead predicted values and the MPC optimized values for the switching power and SOC of the ESS are 8.69% and 0.18%, respectively. The MPC optimum values are consistent with the predicted values, indicating that the rolling control strategy based on MPC can suppress the effects induced by DER fluctuations.

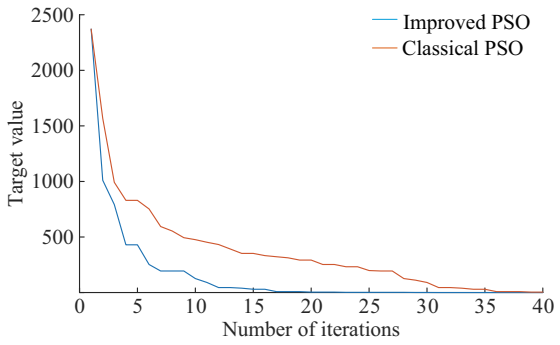

Fig. 5. Convergence curves of classical and algorithms.

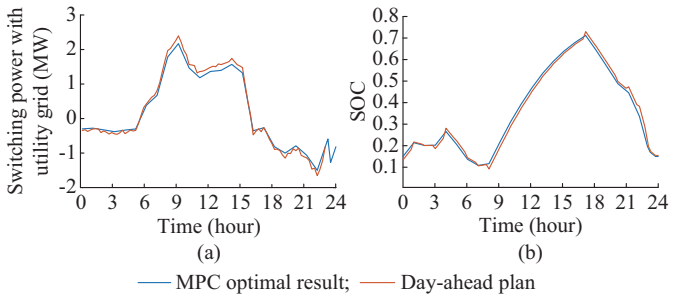

Fig. 6. Optimization results of intraday MPC. (a) Switching power tracing chart. (b) SOC tracing chart.

VI. Conclusion

DC power grids based on flexible high-voltage DC technology have become a common means of facilitating the large-scale integration of DERs and the construction of advanced urban power grids. In the present study, a typical topology for an advanced urban MVDC distribution network with DERs, including wind, PV, and electrical energy storage elements, is analyzed, and a multi-time scale OPF strategy for the MVDC network in the utility grid-connected and off-grid operation modes is proposed. In the utility grid-connected operation mode, the day-ahead optimization objective minimizes both D_{loss} and P_{loss}. However, in the off-grid operation mode, the day-ahead optimization objective gives priority to the minimization of L_{loss} and secondly minimizes D_{loss} and P_{loss}. A dynamic weighting method is employed to transform the multi-objective optimization problem into a QCQP problem that is solvable via standard methods. During intraday scheduling, the optimization objective gives priority to ensure minimum deviation between the actual value and the predicted value of the SOC for the ESS and secondly seeks to minimize D_{loss} and P_{loss}. We adopt MPC to correct deviations according to the results of ultra-short-term load forecasting. An improved PSO algorithm is developed for performing the intraday global optimization, which reduced the computation time to obtain solutions and avoided being trapped in local optima. Finally, MATLAB simulation results indicate that the proposed optimization strategy is effective and efficient.

APPENDIX A

TABLE AI
DATA FOR MVDC DISTRIBUTION NETWORK SCENARIO

Node	Source and load	Capacity (MW)	Input voltage (V)	Output voltage (V)
P1	DC power station	30	±35000	±10000
P2	Subway power supply	5	±10000	±750
P3	Wind farm	10	±750	±10000
P4	Residential area power station	5	±10000	±750
P5	ESS station	5	±750	±10000
P6	PV power station	10	±750	±10000
P7	Industrial park power station	5	±10000	±750
P8	AC power station	30	35000	±10000

TABLE AII
LINE PARAMETERS FOR MVDC DISTRIBUTION NETWORK

No.	Start node	Reach node	Line inductance per unit	Line impedance per unit
1	1	2	0.075	0.10
2	2	3	0.110	0.10
3	1	5	0.110	0.10
4	5	6	0.090	0.10
5	6	7	0.080	0.10
6	7	8	0.070	0.10
7	8	4	0.080	0.10
8	3	4	0.080	0.10

APPENDIX B

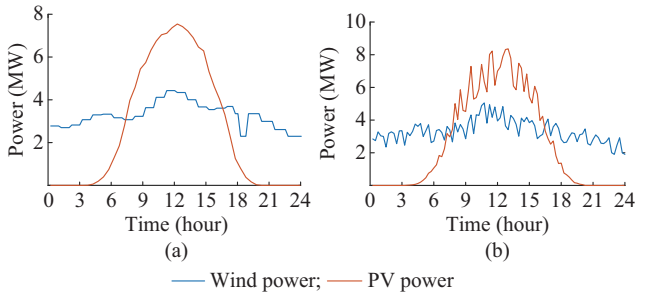

Fig. B1. Day-ahead and intraday forecasting data for DERs. (a) Day-ahead forecasting chart. (b) Intraday forecasting chart.

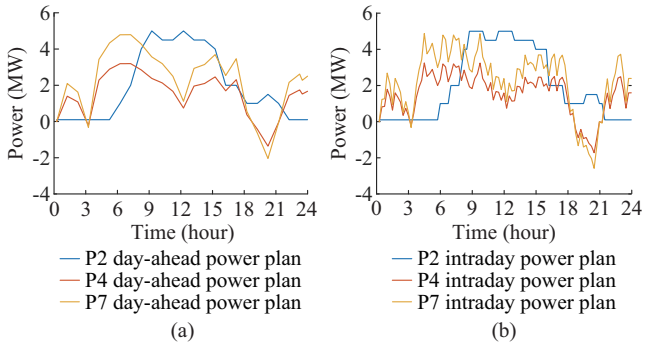

Fig. B2. Day-ahead and intraday forecasting data of loads. (a) Day-ahead forecasting chart. (b) Intraday forecasting chart.

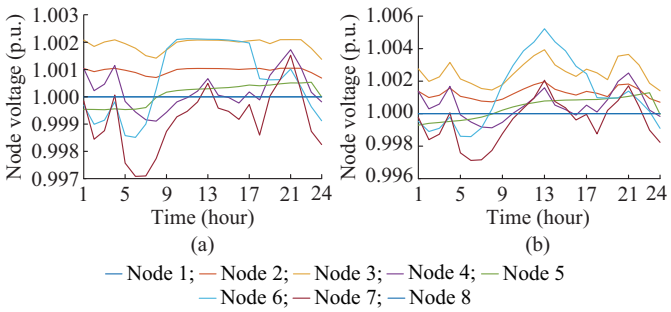

Fig. B3. Node voltages obtained for different weight coefficients employed in Fig. 3. (a) $\lambda_1 = 0.5$, $\lambda_2 = 0.5$. (b) $\lambda_1 = 0.9$, $\lambda_2 = 0.1$.

REFERENCES

[1] L. Yang, "Research on multi-time scale DC distribution network regulation technology," Ph.D. dissertation, North China Electric Power University, Beijing, 2017.

[2] Y. Liu, P. Jing, G. Li *et al.*, "Research on the structure and implementations of the DC grid power control," *Proceedings of the CSEE*, vol. 35, no. 15, pp. 3803-3814, Aug. 2015.

[3] X. Li, L. Guo, C. Wang *et al.* "Key technologies of DC microgrids: an overview," *Proceedings of the CSEE*, vol. 36, no. 1, pp. 2-17, Jan. 2016.

[4] X. Liu, J. Wen, Y. Pan *et al.*, "OPF control of DC-grid using improved PSO algorithm," *Power System Technology*, vol. 41, no. 3, pp. 715-720, Mar. 2017.

[5] H. Xiao, W. Pei, and L. Kong, "Multi-time scale coordinated optimal dispatch of microgrid based on model predictive control," *Automation of Electric Power Systems*, vol. 40, no. 18, pp. 7-14, Sept. 2016.

[6] S. Yang, J. Liu, J. Yao *et al.*, "Model and strategy for multi-time scale coordinated flexible load interactive scheduling," *Proceedings of the CSEE*, vol. 34, no. 22, pp. 3664-3673, Aug. 2014.

[7] S. Guo, Y. Yuan, X. Zhang *et al.*, "Energy management strategy of isolated microgrid based on multi-time scale coordinated control," *Transactions of China Electrotechnical Society*, vol. 29, no. 2, pp. 122-129, Feb. 2014.

[8] H. Xu, Y. Li, S. Miao *et al.*, "Optimization dispatch strategy considering renewable energy consumptive benefits based on 'source-load-energy storage' coordination in power system," *Power System Protection and Control*, vol. 45, no. 17, pp. 18-25, Sept. 2017.

[9] H. Moradi, D. D. Groff, and A. Abtahi, "Optimal energy scheduling of a stand-alone multi-sourced microgrid considering environmental aspects," in *Proceedings of 2017 IEEE PES Innovative Smart Grid Technologies Conference*, Washington DC, USA, Apr. 2017, pp. 1-5.

[10] D. Bosich, A. Vicenzutti, and G. Sulligoi, "Robust voltage control in large multi-converter MVDC power systems on ships using thyristor interface converters," in *Proceedings of 2017 IEEE Electric Ship Technologies Symposium*, Arlington, USA, Aug. 2017, pp. 267-273.

[11] I. Kondratiev and R. Dougal, "Synergetic control strategies for shipboard DC power distribution systems," in *Proceedings of the 2007 American Control Conference*, New York, USA, Jul. 2007, pp. 4744-4749.

[12] D. Mildt and R. Kubo, "Decentralized hybrid switching control of multi-converter MVDC shipboard power systems," in *Proceedings of 43rd Annual Conference of the IEEE Industrial Electronics Society*, Beijing, China, Oct.-Nov. 2017, pp. 6795-6800.

[13] F. Mura, and R. W. D. Doncker, "Design aspects of a medium-voltage direct current (MVDC) grid for a university campus," in *Proceedings of 8th International Conference on Power Electronics - ECCE Asia*, Jeju, South Korea, May-Jun. 2011, pp. 2359-2366.

[14] P. Kankanala, S. C. Srivastava, A. K. Srivastava *et al.*, "Optimal control of voltage and power in a multi-zonal MVDC shipboard power system," *IEEE Transactions on Power Systems*, vol. 27, no. 2, pp. 642-650, May 2012.

[15] M. Baradar, M. R. Hesamzadeh, and M. Ghandhari, "Modelling of multi-terminal HVDC systems in optimal power flow formulation," in *Proceedings of 2012 IEEE Electrical Power and Energy Conference*, London, UK, Oct. 2012, pp. 170-175.

[16] L. T. D. Santos, M. Sechilariu, and F. Locment, "Day-ahead microgrid optimal self-scheduling comparison between three methods applied to isolated DC microgrid," in *Proceedings of 40th Annual Conference of the IEEE Industrial Electronics Society*, Dallas, USA, Oct.-Nov. 2014,

pp. 2010-2016.
[17] Y. Zhang, K. Gao, Z. Han *et al.*, "Multi-objectives OPF of AC-DC systems considering VSC-HVDC integration," in *Proceedings of 2016 IEEE PES Asia-Pacific Power and Energy Engineering Conference*, Xi'an, China, Oct. 2016, pp. 929-933.
[18] W. Liu, S. Niu, and H. Xu, "Optimal planning of battery energy storage considering reliability benefit and operation strategy in active distribution system," *Journal of Modern Power Systems and Clean Energy*, vol. 5, no. 2, pp. 177-186, Mar. 2017.
[19] P. Song, Z. Xu, H. Dong *et al*., "Security-constrained line loss minimization in distribution systems with high penetration of renewable energy using UPFC," *Journal of Modern Power Systems and Clean Energy*, vol. 5, no. 6, pp. 876-886, Nov. 2017.
[20] H. Yu, C. Zhang, Z. Deng *et al*., "Economic optimization for configuration and sizing of micro integrated energy systems," *Journal of Modern Power Systems and Clean Energy*, vol. 6, no. 2, pp. 330-341, Mar. 2018.
[21] B. Zhao, Z. Hu, Q. Zhou *et al*., "Optimal transmission switching to eliminate voltage violations during light-load periods using decomposition approach," *Journal of Modern Power Systems and Clean Energy*, vol. 7, no. 2, pp. 297-308, Mar. 2019.

Jianqiang Liu received the B.S. and Ph.D. degrees in electrical engineering from Beijing Jiaotong University, Beijing, China, in 2003 and 2008, respectively. Presently, he is a professor in the School of Electrical Engineering, Beijing Jiaotong University. His research interests include electric energy conversion, control of AC machines, and traction drive system.

Xiaoguang Huang received the B.S. and M.S. degrees in electrical engineering from Beijing Jiaotong University, Beijing, China, in 2001 and 2006, respectively, where he is currently working toward the Ph.D. degree. His research interests include optimal dispatch of power system, smart grids and energy hubs.

Zuyi Li received the B.S. degree from Shanghai Jiao Tong University, Shanghai, China, in 1995, the M.S. degree from Tsinghua University, Beijing, China, in 1998, and the Ph.D. degree from the Illinois Institute of Technology (IIT), Chicago, USA, in 2002, all in electrical engineering. He is currently a professor with the Electrical and Computer Engineering Department, IIT, Chicago, USA. His research interests include economic and secure operation of electric power systems, cyber security in smart grid, renewable energy integration, electric demand management of data centers, and power system protection.